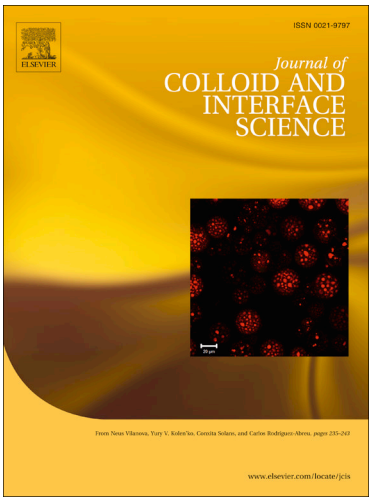
CORA Cork Open Research Archive
Cartlann Taighde Oscailte Chorcaí

| | |
|---|---|
| Title | Fabrication of Si and Ge nanoarrays through graphoepitaxial directed hardmask block copolymer self-assembly |
| Authors | Gangnaik, Anushka S.;Ghoshal, Tandra;Georgiev, Yordan M.;Morris, Michael A.;Holmes, Justin D. |
| Publication date | 2018-06-30 |
| Original Citation | Gangnaik, A. S., Ghoshal, T., Georgiev, Y. M., Morris, M. A. and Holmes, J. D. (2018) 'Fabrication of Si and Ge nanoarrays through graphoepitaxial directed hardmask block copolymer self-assembly', Journal of Colloid and Interface Science. doi:10.1016/j.jcis.2018.06.018 |
| Type of publication | Article (peer-reviewed) |
| Link to publisher's version | 10.1016/j.jcis.2018.06.018 |
| Rights | © 2018, Elsevier Inc. All rights reserved. This manuscript version is made available under the CC-BY-NC-ND 4.0 license. - https://creativecommons.org/licenses/by-nc-nd/4.0/ |
| Download date | 2026-11-06 13:28:16 |
| Item downloaded from | https://hdl.handle.net/10468/6446 |

UCC
University College Cork, Ireland
Coláiste na hOllscoile Corcaigh

Accepted Manuscript




# Fabrication of Si and Ge nanoarrays through graphoepitaxial directed hardmask block copolymer self-assembly

Anushka S. Gangnaik, Tandra Ghoshal, Yordan M. Georgiev, Michael A. Morris, Justin D. Holmes

PII: S0021-9797(18)30666-0
DOI: https://doi.org/10.1016/j.jcis.2018.06.018
Reference: YJCIS 23709

To appear in: *Journal of Colloid and Interface Science*

Received Date: 7 February 2018
Revised Date: 5 June 2018
Accepted Date: 6 June 2018

Please cite this article as: A.S. Gangnaik, T. Ghoshal, Y.M. Georgiev, M.A. Morris, J.D. Holmes, Fabrication of Si and Ge nanoarrays through graphoepitaxial directed hardmask block copolymer self-assembly, *Journal of Colloid and Interface Science* (2018), doi: https://doi.org/10.1016/j.jcis.2018.06.018

This is a PDF file of an unedited manuscript that has been accepted for publication. As a service to our customers we are providing this early version of the manuscript. The manuscript will undergo copyediting, typesetting, and review of the resulting proof before it is published in its final form. Please note that during the production process errors may be discovered which could affect the content, and all legal disclaimers that apply to the journal pertain.

ACCEPTED MANUSCRIPT

# Fabrication of Si and Ge nanoarrays through graphoepitaxial directed hardmask block copolymer self-assembly

Anushka S. Gangnaik,[a,b*] Tandra Ghoshal,[a,b] Yordan M. Georgiev,[a,b] Michael A. Morris,[a,b] Justin D. Holmes [a,b]

[a,b]School of Chemistry and Tyndall National Institute, University College Cork, Cork, Ireland

[*] Corresponding Author:

Tandra Ghoshal

Tel: + 353 21 490 2911

Fax: +353 21 427 4097

E-mail: g_tandra@yahoo.co.in

ACCEPTED MANUSCRIPT

ACCEPTED MANUSCRIPT

**ABSTRACT**

Films of self assembled diblock copolymers (BCPs) have attracted significant attention for generating semiconductor nanoarrays of sizes below 100 nm through a simple low cost approach for device fabrication. A challenging abstract is controlling microdomain orientation and ordering dictated by complex interplay of surface energies, polymer-solvent interactions and domain spacing. In context, microphase separated poly (styrene-*b*-ethylene oxide) (PS-*b*-PEO) thin films is illustrated to fabricate nanopatterns on silicon and germanium materials trenches. The trenched templates was produced by simple electron beam lithography using hydrogen silsesquioxane (HSQ) resist. The orientation of PEO, minority cylinder forming block, was controlled by controlling trench width and varying solvent annealing parameters viz. temperature, time etc. A noticeable difference in microdomain orientation was observed for Si and Ge trenches processed under same conditions. The Ge trenches promoted horizontal orientations compared to Si due to difference in surface properties without any prior surface treatments. This methodology allows to create Ge nanopatterns for device fabrication since native oxides on Ge often induce patterning challenges. Subsequently, a selective metal inclusion method was used to form hardmask nanoarrays to pattern transfer into those substrates through dry etching. The hardmask allows to create good fidelity, low line edge roughness (LER) materials nanopatterns.

Keywords: Germanium, nanopatterns, self-assembly, trench, pattern transfer

ACCEPTED MANUSCRIPT

ACCEPTED MANUSCRIPT

## 1. Introduction

Since the beginning of 21st century, the improved performance of microelectronic devices showed signs of slowdown, largely due to limitations arising from patterning tools [1]. In order to deliver further device miniaturisation, methods and equipment must be fashioned to allow material engineering at the molecular level. Bottom-up technologies are an instinctive alternative to traditional top-down lithography for a cost-effective device design, which mainly involves the use of various polymers. They involve simpler processes of lithographic technology and furthermore, they are comparatively cheaper option since they do not require expensive facilities or equipment. Lithography with polymeric materials is also compatible with existing integrated circuits technology since they are with chemically similar composition to photo or electron beam lithography (EBL) resists. Nanoscale polymer features are obtained from their molecular constituents that are driven to self-assembly by kinetic processes or thermodynamic forces [2]. The term self-assembly defines the spontaneous and regular arrangement of nanoscale units in order to attain a minimum Gibbs energy by minimising the repulsive and maximising the attractive molecular interactions [3].

Block copolymers (BCP) have great potential as etch masks in the fabrication of semiconductor nanopatterns due to their molecular scale precision, ultrafine line edge roughness (LER), and low-cost processing [4-6]. BCPs are a special class of polymers where two or more distinct homopolymers subunits are polymerised to produce covalent bonding between BCP chains [5]. Due to this chemical dissimilar nature, the polymer segments phase separate on the nanometre scale under certain conditions [7].

ACCEPTED MANUSCRIPT

By varying the molecular weights of the polymer blocks and the interfacial energies, excellent control over the BCP domain shape (lamella, spherical, cylindrical or gyroidal) and sizes can be achieved. Once the desired orientation is achieved, one of the blocks can be selectively removed and the remaining pattern can be transferred into the desired functional device material [8-10]. Moreover, many strategies have been investigated to manipulate interfacial interactions, to obtain a specific orientation and/or lateral ordering of the microdomains including external fields (magnetic, electrical), sample temperature gradient, mechanical effects such as rubbing and substrate topographical and chemical patterns [11-14]. BCP lithography therefore has the potential to be used to fabricate high density, well-ordered arrays of functional nanostructured materials on substrate surfaces, which is not only scientifically interesting but also a technologically important area; due to potential applications in nanoelectronics, optoelectronics, information storage, photonics, catalysis and sensors [8, 11-12].

One of the major challenges in using BCPs for nanofabrication is the lack of long range periodic ordering of the polymer segments on a substrate. Directed self-assembly (DSA) of BCPs can be achieved however by introducing topographic guiding features such as trenches or pillars on the substrate surface. These topographic pre-patterns have been reported to effectively monitor and improve the ordering of some of the BCP systems [13-15]. This category of lithography is known as directed self-assembly by graphoepitaxy. A considerable amount of research has been undertaken to optimise the DSA of BCPs. The DSA of lamellar forming poly(styrene b-methyl methacrylate) (PS-b-PMMA) using EBL to produce simple hydrogen silsesquioxane (HSQ) line patterns that act as guides for BCPs has been reported [16]. EBL exposed dot patterns have also been used for administrating the

ACCEPTED MANUSCRIPT

self-assembly of spheres forming BCP from poly(styrene-b-dimethlysiloxane) (PS-b-PDMS) which were explored for bit-patterned media with a density of around 1.5 teradots/inch$^2$ [17]. Other instances of using EBL-patterned HSQ for guiding BCP orientation has also been reported [18]. Besides graphoepitaxy, chemical pre-treatment of the surface prior to BCP deposition is also another DSA approach, wherein a brush layer is deposited on the substrate prior to BCP processing [19].

In this article, a method to generate highly ordered Si and Ge nanopatterns, aligned with the help of simple HSQ gratings fabricated by EBL, via a simple and cost-effective in-situ BCP hard mask inclusion technique is demonstrated. The nanofabrication process is based on the use of solvent-induced microphase separation in PS-b-PEO thin films; where the marked difference in the chemical functionality of the PS and PEO blocks allows selective metal ion inclusion [20]. The structural and morphological variation in the BCP phase separated patterns can be achieved by changing the solvent annealing time and temperature, the width and spacing between the gratings and pre-treatment of substrate surface. Unlike several BCP/substrate systems, the PS-b-PEO system does not require any homopolymer brush layer deposition and any pre surface modification of the substrate. Iron oxide nanopatterns were fabricated from the assembled PS-b-PEO nanopatterns through an in-situ inclusion technique, which were subsequently used as hardmask to transfer nanopatterns into Si or Ge trenched substrates [21].

## 2. Experimental section

### 2.1. Graphoepitaxy process for the fabrication of Si and Ge trenches

Scheme 1 represents the schematic description of the graphoepitaxy process for the fabrication of Si and Ge trenches on substrate surface. Si or Ge substrates of 10 × 10 mm were diced from a <100> orientation Si or Ge wafer, respectively and used

ACCEPTED MANUSCRIPT

throughout the experiment. The substrates were first degreased by ultrasonication in acetone and subsequently in isopropyl alcohol (IPA) for 120 s. The Si substrates were dried with a $N_2$ gun and then by baking at a temperature of 120 °C for 180 s. They were then patterned using the hydrogen silsesquioxane (HSQ) high-resolution EBL resist. A 2.4 wt % solution of HSQ in methyl isobutyl ketone was spin-coated onto a Si substrate a 2000 rpm for 33 s to give a thin film resist thickness of approximately 50 nm (Scheme 1(a)). After spin coating, the substrate was baked at a temperature of 120 °C for 180 s on a hotplate prior to EBL (Raith e-Line Plus) exposure. Arrays of 50 nm wide lines were exposed at 10 kV having pitch sizes of (45n+50) where $0 < n < 7$. After the EBL exposure, the substrates were developed by immersion in an aqueous mixture of 0.25 M NaOH, 0.7 M NaCl for 15 s, followed by a 60 s rinse in DI water and then 15 s dip in IPA solution. Subsequently, the substrates were blown dry in flowing $N_2$ gas. Thus, high resolution HSQ gratings were achieved (Scheme 1(b)). In the case of Ge substrates, after the IPA and acetone cleaning they were processed in a different way prior to EBL patterning. Due to the presence of the native oxides on the Ge surface, each substrate was passivated by immersing the Ge substrates in 1.73 M citric acid. HSQ resist was spin-coated onto the Ge substrates and administered in the same manner as detailed above. Citric acid treatment ensured the adhesion of HSQ resist after developing the resist with aqueous developer solutions.

2.2. BCP microphase separation and hardmask nanopattern formation process

PS-b-PEO powder (Polymer Source) was dissolved in toluene at room temperature and aged for 12 h to prepare a 0.4 wt% solution. The molecular weight ($M_n$) of the BCP was PS = 42 kg/mol, and PEO = 11.5 kg/ mol, $M_w/M_n = 1.07$, where Mw and $M_n$ is the weight and number-average molecular weight. Thin films of BCP were deposited on the Si and Ge trench substrates by spin-coating the polymer solution with

ACCEPTED MANUSCRIPT

3000 rpm for 30 s (Scheme 1(c)). The substrates were then placed in a sealed jar and exposed to toluene vapour. The films were annealed for various time periods at 50 or 60 °C to induce mobility and commence microphase separation (Scheme 1(d)). After the solvent annealing, the Si chips were immersed in ethanol solution for 15 h at 40 °C, resulting in partial modification of one of the BCP blocks, i.e. the PEO block (Scheme 1(e)). For the fabrication of the metal oxide hardmask, different concentrations of iron (III) nitrate nonahydrate ($Fe(NO_3)_3 \cdot 9H_2O$) were dissolved in anhydrous ethanol and was spin-coated onto the patterned substrates (Scheme 1(f)). The substrates were subsequently subjected to UV/ozone oxidation (PSD Pro Series Digital UV Ozone System; Novascan Technologies, Inc., USA) to oxidise to form iron oxide mask on the substrates (Scheme 1(g)).

2.3. Fabrication of Si and Ge nanopatterns within trenches

These iron oxide nanopattern arrays were used as a hard mask for pattern transfer to the substrate using the Surface Technology Systems (STS) Inductively Coupled Plasma (ICP) Etcher (Multiplex ICP) system (Scheme 1(h)) [15-16]. A double etching process was used to, firstly, etch the native silica layer and, secondly, the Si itself, in the case of Si substrates. During etching, the sample was thermally bonded to a cooled chuck (10°C) with a pressure of 9.5 mTorr. For the oxide layer etch, the process parameters were optimised to a $C_4F_8/H_2$ gas mixture (21 sccm/30 sccm). The silica etch time was kept constant (5 s) for all the samples. For Si etching, the process used a controlled gas mixture of $C_4F_8/SF_6$ at flow rates of 90 sccm/30 sccm respectively and the ICP and RIE powers were set to 600 and 15 W respectively, at a chamber pressure of 15 mTorr. Likewise, in the case of Ge, STS etcher was used to transfer the metal oxide nanowire mask pattern to the underlying GeOI/Ge substrate. $CF_4$ and $C_4F_8$ gases were used for etching Ge with the metal oxide nanostructures as

ACCEPTED MANUSCRIPT

etch masks. Samples were etched for various times using a flow rate of 40 sccm, pressure of 10 mTorr, and ICP power of 400 W.

2.4. Characterizations

Surface morphologies were imaged by scanning electron microscopy (SEM, FEI Company, FEG Quanta 6700 and Zeiss Ultra Plus) at 10 kV and 5 kV. Samples were prepared for TEM cross sectional imaging with an FEI Helios Nanolab 600i system containing a high resolution Elstar™ Schottky field-emission SEM and a Sidewinder FIB column and were further imaged by transmission electron microscopy (TEM, JEOL 2100).

## 3. Results and Discussion

3.1. Microphase separation of BCP on Si and Ge substrates

HSQ gratings on Si and Ge substrates patterned by EBL act as guiding templates for the self-assembly of the BCP system. The BCP employed in this study was PS-b-PEO (42k-11.5k), with PEO as the minority cylinder forming block. The HSQ trench widths were varied in the range of multiples of 45 nm so as to accommodate BCP patterns within them because the cylinder-cylinder spacing and the PEO microdomain diameter were ~ 42 nm and ~ 19 nm respectively. The depth of the trenches was fixed at 50 nm that is the thickness of HSQ resist film. Fig. 1a shows a high magnification SEM image of arrays of HSQ lines forming the trench prior to deposition of BCP on Si. BCP nanopatterns were created by spin-coating the polymer solution onto the trenched substrates followed by solvent vapour annealing at different temperatures and time. Note that the concentration of the polymer solution was calibrated to avoid overfilling of BCP within the trenches. For all the experimental conditions studied, a 0.4 wt% BCP-toluene solution was used. The structural arrangement of the PS and PEO blocks for the solvent annealed films after the phase separation could not be determined by SEM due to the lack of electron contrast between the blocks. All the

ACCEPTED MANUSCRIPT

films were subjected to anhydrous ethanol treatment for a certain period of time to enhance the electron contrast between them which partially etch and/or modify the PEO domains. These ethanol treated films were then studied by SEM to investigate the BCP nanopatterns. Periodic arrangements of the BCP with PEO cylinders oriented perpendicularly to the substrate surface inside the PS matrix were obtained on an open surface area over the Si substrate where the HSQ gratings were not present after solvent annealing at a temperature of 50 °C for 2 h, as shown in Fig. 1b. Similarly, Fig. 1c shows the BCP self-assembled line patterns with parallel orientation of the PEO cylinders inside the PS matrix on the open area of the Ge substrate. Structural and orientational variation of the same BCP for two different substrates is evident from the SEM images in Figs. 1b and c under the similar processing parameters. The Ge surface mainly promoted the parallel orientation of the PEO cylinders with line patterns, although perpendicularly oriented dot patterns were also noticed at various areas on Si substrates.

### 3.2. Microphase separation of BCP on HSQ trenched Si and Ge substrates

Successively, the BCP self-assembly was observed in the HSQ trenches on Si and Ge surface and the experimental parameters were varied to achieve an optimum nearly defect free nanopatterns with desired microdomain orientation. Fig. 2 shows the DSA of PS-b-PEO within HSQ trenches, annealed for 2 h at two different temperatures. The polymer uniformly wetted the substrate surface without any ordered structure for the wider trench widths (> 135 nm) before the solvent annealing process (not shown). SEM images in Fig. 2a and b displays the BCP dot patterns (PEO cylinders perpendicularly orientated inside PS matrix) within HSQ trenches on the Si substrate solvent annealed at 50 °C for 1.5h and 60 °C for 2 h, respectively. The solvent annealing time were varied to achieve vertically oriented cylindrical PEO

ACCEPTED MANUSCRIPT

microdomains from 1.5 to 2 h with increasing the temperature. Fig. 2a shows the SEM image of the BCP dots within 90 nm HSQ trench over large areas with no or little de-wetting. Subsequently, the annealing temperature was increased to 60 °C without changing other experimental parameters. An ordered, aligned arrangement of a set of array of hexagonally arranged dot patterns were also observed within 135 nm trenches, but thickness variations and/or pattern degradation was noticed in a few places as in Fig. 2b. The number of arrays of dots increased with increasing trench width. The mean measured centre-to-centre distance between adjacent microdomains was 42 nm, whereas the PEO cylinder diameter was around 19 nm for both trench widths. In the case of Ge, when the BCP films were solvent annealed in toluene for 1h 30 min, BCP dot patterns with perpendicular cylinder orientation were noticed within the trenches, similar to that on Si surface. However, when the films were annealed for longer time to 2 h, parallel orientation of PEO cylinders were observed within HSQ trenches wider than 180 nm. In smaller trenches (<135 nm), viz. 45 and 90 nm, only dot patterns were observed. Both perpendicular and parallel orientation of PEO cylinders were realized for the HSQ trench width of 135 nm (not shown here). Nearly defect free, long range ordered parallel PEO cylinders arrangement of array of BCP line patterns were observed for the wider HSQ trenches (225 to 315 nm) on the Ge substrate, as shown in Fig. 2c and Fig.2d respectively. The number of arrays also increases with increasing the trench width. Similar BCP nanopatterns were achieved for the temperature of 60 °C within HSQ trenched Ge substrates.

3.3. BCP nanopatterns on HSQ etched Si and Ge trenched substrates

The trenched substrate surfaces were modified to achieve well-ordered nearly defect free periodic features within the trenches. An etching step achieved by RIE using Cl-chemistry for 25 sec was used to remove the HSQ layer [22]. A Solvent annealing

ACCEPTED MANUSCRIPT

temperature of 60°C for 2 h was applied to achieve BCP patterns within HSQ etched Si trenches (50 nm depth). No microphase separation or patterns was achieved for the smallest trench width of 45 nm although well-ordered arrays of patterns were observed for all of the wider Si trenches. Furthermore, BCP wetted the trench uniformly and contrast enhancement was also noticed. Increasing the trench width to 90 nm, a single array of a combination of parallel and perpendicular orientated PEO cylinders inside the PS matrix was observed. Fig. 3a shows large scale area BCP nanopatterns for 2 μm long and 90 nm wide trenches. The PEO cylinders (darker contrast) resides almost in the middle of the trenches, whereas PS wetted the sidewalls. As the trench width was increased, the wetting preference was governed by the surface energy. Similar mixed orientations of the cylinders was realized for the wider trench of 135 nm and 180 nm. Further increases in the trench widths resulted in perpendicular orientation of the cylinders only near the edges of the trenches, as shown in Fig. 3b for 270 nm wide trenches. No patterns were realized in the intermediate areas for the wider trenches and additionally, frequent defects were observed. Thus, HSQ etching does not significantly improves the quality and uniformity of the BCP nanopatterns within Si trenches.

Arrays of well-ordered periodic dot patterns were realised for the HSQ etched Ge trenches where PEO cylinders oriented perpendicular to the substrate surface for the annealing temperature of 60 °C for 2 h irrespective of trench width. Figs. 3c and d shows two and six arrays (two of them alongside the edges) of dots for the 135 nm and 270 nm wide HSQ etch Ge trench. No parallel orientations of the PEO cylinders were observed. The number of arrays of dots increases with increasing trench widths. Few defects were observed with increasing the trench width to 270 nm or above.

### 3.4. BCP nanopatterns on UV/Ozone treatment modified HSQ trenched Si substrate

ACCEPTED MANUSCRIPT

To further improve the quality of the BCP nanopatterns within the Si trenches, a UV/Ozone treatment process was followed prior to BCP deposition. To modify the substrate chemistry and to achieve the parallel orientation of PEO cylinders, the HSQ trenched Si substrates were exposed to UV/Ozone treatment for 30 min before spin-coating the BCP solution. The BCP solution was spin coated within 5 minutes of UV/Ozone treatment to prevent further oxidation within trenches.

This step makes the surface more hydrophilic; the water contact angle for Si is reported to be 21°, whereas after UV/Ozone treatment the contact angle was found to be 90° [23]. A hydrophilic Si surface promotes the formation of Si-OH bonds which increases the affinity for the PEO block for both the trenches and the HSQ sidewalls. After spin-coating the BCP films, the substrates were solvent annealed for 1.5 h and 2 h at 60 °C. Figs. 4a and b show the microphase separated BCP nanopatterns for U/Ozone treated HSQ defined Si trenches for 225 nm (1.5 h annealing time) and 90 nm (2h annealing time) trench widths, respectively. No patterns were observed for the smaller trench widths (45 nm). Well-ordered arrays of dots were noticed for an annealing time of 1.5 h in 225 nm trenches whereas line patterns achieved for 2h annealing time for narrower trench. The HSQ templates were, however, affected by the U/Ozone treatment, as observed from both the images in Fig. 4. In a few places, pattern degradation and/or swelling (pointed out by the red circles) was noticed with similar translational order and feature sizes, though dot patterns were predominant, shown in Fig. 4(a). Poorly ordered nanopatterns and swelling of the PEO microdomains became more prominent with further increase in the trench widths. On comparing Figs. 4a and b, the obvious difference is seen in the orientation of the BCP. Long range well-ordered PEO cylinders parallel to the substrate in the PS matrix were observed for 90 nm wider trench with increasing the annealing time to 2 h. Two

ACCEPTED MANUSCRIPT

continuous arrays of BCP line patterns for more than 3 μm long trench can be seen. The arrays were continuous with the PEO cylinders parallel to the trench surface, whereas the PS wets the sidewalls, as seen from the inset of Fig. 4b. The cylinder-to-cylinder spacing and cylinder diameter remains the same as was observed for the dot patterns. However, as mentioned above the HSQ lines did not adhere on the substrate and it can be presumed that the ozone treatment must have initiated the HSQ removal since this effect was not observed in non-UV/ozone treated substrates.

### 3.5. BCP nanopatterns on citric acid modified HSQ trenched Ge substrates

Native oxides on Ge surface usually interfere the BCP patterning because of modification in the interfacial energies and therefore UV/ozone treatment of Ge would not be beneficial for device fabrication. The subsequent procedures were followed to remove the native oxides on Ge by treating them with 1 M citric acid prior to spin coating of the BCP thin film. The acid treatment ensured an oxide-free surface, thus passivating the substrate with the citric acid was performed for the trenched Ge substrates. Fig. 5a shows an SEM image of the self-assembled BCP thin film on a Ge substrate on the open area after solvent annealing at 60 °C for 2h. BCP dot patterns with perpendicularly oriented PEO cylinders was realized over the entire substrate area with cylinder to cylinder spacing of 42 nm. Defects in terms of pattern degradation/missing is also evident. Figs. 5b and c displays the BCP nanopatterns within 135 nm and 270 nm citric acid modified HSQ guided Ge trenches respectively. Similarly ordered arrays of dots were observed. For smaller trench widths, parallel orientation of cylinders was realised in a few areas although the perpendicular orientation was predominant. All of the wider trenches (225, 270 and 315 nm) produced PEO cylinders with perpendicular orientation, in contrast to the parallel orientation observed for the same trench width on the untreated HSQ guided Ge

ACCEPTED MANUSCRIPT

trenches. When the Ge surface was treated with citric acid, citrate ions are probably adsorbed onto the surface giving it a negative zeta potential (depending on the citric acid concentration) [24]. This acid passivation may change the surface energy of Ge and does not favour long range parallel arrangement of the microdomains on Ge surface.

### 3.6. Formation of iron oxide nanopatterned hardmask on Si and Ge trenched substrates

The BCP nanopatterns formed were used as a template to create ordered oxide nanostructures by an in-situ metal ion inclusion method [25]. The precursor iron (III) nitrate nonahydrate - anhydrous ethanol solution (0.4 wt.%) was spin-coated onto the nanoporous polymer templates within the trenches and subjected to UV/Ozone treatment. The UV/Ozone treatment ensured the formation of iron oxide nanopatterns and removal of polymers. The iron oxide nanopatterns were then used as a hardmask for transferring the pattern into the substrates. In order to create well-ordered arrays of nanodots or nanowires, the best quality BCP nanopatterns substrates were chosen, i.e. films annealed at 60 °C for 1.5 h with HSQ-etched Si trenches for the dots and films annealed at 60 °C for 2 h with UV/Ozone treated HSQ trenched Si and Ge substrate for the nanowires.

Fig. 6a represents the SEM images of iron oxide nanodots and lines patterns prepared after UV/Ozone treatment (3 h) on an open area Ge substrate. The precursor concentrations were adjusted to achieve well-ordered iron oxide arrays of well-separated nanodots and continuous defect-free nanowires within the trenches. At a precursor concentration of 0.4 wt%, well-ordered arrays of iron oxide nanodots/lines arrays were obtained. Fig. 6b shows metal oxide dots within 135 nm sized HSQ trenches of Si, highlighting that the average diameter of the iron oxide nanodots around 23 nm whereas the centre-to-centre nanodots spacings (~ 42 nm) are equivalent

ACCEPTED MANUSCRIPT

to that of the BCP domain. Fig. 6c illustrates iron oxide nanolines obtained by the metal inclusion process on the HSQ trenched Ge substrate. The measured diameter and spacing of the line structures were ~23 nm and 42 nm respectively comparable to the dot patterns on Si substrates. The concentration of the iron precursor solution was critical and carefully optimised to obtain isolated and continuous nanowires [25]. Due to the hydrophobic nature of PS, the probability of the metal ion inclusion into the PS matrix was excluded; thereby metal ions occupy PEO activated sites. During the UV/Ozone treatment, the metal crosslinks with the BCP blocks, removes the organic compounds present in the solvent and polymers as a volatile compound and further oxidizes the iron precursor. One of the main reasons for carrying out the ethanol treatment erstwhile is that during the deposition of metal oxide the remaining hydrophilic PEO within the polymer template will aid in the absorption of the metal ions into the PEO voids. This is because PEO swells during ethanol treatment and later due to affinity of PEO with the cations, the incorporation of metal ions within the pores will speed up [26]. The oxygen atoms present in the activated PEO microdomains chemically coordinate with the metal ions by intermolecular force of attraction. After this process, iron oxide ($Fe_3O_4$) nanodots and nanowires were formed as shown in Fig. 6 [25].

### 3.7. Fabrication of Si nanopillars within trenches

Fig. 7 illustrates Si nanopillars obtained after pattern transfer using iron oxide hardmask on Si trenches. The contrast enhancement compared to the SEM image shown in Fig. 6b confirming that pattern transfer via this route was successful and providing evidence of the mechanical robustness of the hardmask. The depth of the nanorods/wires could be varied by increasing the Si etch time. Fig. 7a reveals well-ordered arrays of Si nanorods within 180 nm wide Si trenches etched for 30 s. A

ACCEPTED MANUSCRIPT

higher magnification cross-sectional SEM image (inset of Fig. 7a) demonstrates the uniform and equal diameter of the nanorods observed for iron oxide nanodots (23 nm). The cross-sectional SEM image also confirms the uniform width and smooth sidewalls throughout the entire length demonstrating the mask effectiveness. The centre-to-centre spacing remained unchanged, implying that the etching did not damage the original 'mask' to a significant extent. The nanopatterns remained unaffected with increasing etch times, further long nanorod patterns were observed. Cross-sectional TEM was used to fully characterise the nanowires. Fig. 7b shows TEM image of a Si nanopillar achieved after a 30 s etch within a 90 nm wider trench, with iron oxide at the top. This image clearly shows Si nanopillars with 10 nm thick HSQ layer and iron oxide nanodot at top. Further, equal diameter and smooth sidewalls can also be accomplished.

### 3.8. Fabrication of Ge nanowires within trenches

An etch step using $CF_4$ gas and an iron oxide hardmask was employed for pattern transfer into the Ge trenches. $CF_4$ gas has previously been reported to transfer poly(styrene-b-4 vinyl pyridine) BCP pattern efficaciously into Ge substrates [26]. Figs. 8a and b illustrate Ge nanostructures formed after etch times of 9 and 6 s etch within 180 nm and 225 nm wide HSQ trench respectively. The inset shows the patterns on open areas on the same substrates. The pattern transfer was realised in both the cases as can be seen from the contrast enhancement but the line patterns become discontinuous. The deterioration is more for longer etch times. Additionally, the roughness of the HSQ side walls can also be noticed in Figs. 8a and b. This roughness could be due to the fact that the $CF_4$ etch chemistry is known to consume HSQ, thus etching it at higher rate than intended and resulting in rougher sidewalls [27]. This etch recipe, or time, proved to overly etch the hard mask and destroyed the

ACCEPTED MANUSCRIPT

lines as well as the dot morphology. In 135 nm wide trenches, discontinuous Ge nanofins laying perpendicular to the HSQ trench were observed for a 6s Ge etch (not shown). In Fig. 8b, 225 nm wide HSQ trenches show up to 4 continuous Ge nanowires parallel to the trenches. However, as evident from Fig. 8b, the etching process resulted in the disruption of the lines and appeared more like nanodots structures. The inset also shows fingerprint Ge nanostructures etched through the iron oxide hard mask. Fig. 8c shows the Ge nanolines that were etched for a shorter time (4 s). It can be clearly seen from the SEM image that 4 s were also harsh, thus conducting that an alternate etch recipe should be employed to this BCP/Ge system.

A different etch step with $C_4F_8$ gas was applied for 9 s to pattern transfer onto the HSQ guided Ge trenches. Fig. 9 shows the nanopatterns within 135 nm wider Ge trench. The SEM image reflects better quality Ge nanowire patterns with diameter ~ 20 nm and spacing of 42 nm. Unlike previous wires, these nanowires were continuous and spanned over the entire area of the trench. Fig. 9b shows the cross sectional TEM image of 5 arrays of Ge nanowire patterns achieved after 9 s etch within a 225 nm wider trench, with HSQ at the sides and iron oxide at the top. The depth of the nanowire is around 35 nm. This clearly shows Ge nanowires with 10 nm thick HSQ layer and iron oxide nanowire at top. The spread of the Ge nanowire diameter was found to be between 17-20 nm.

3.9. Discussion

Previous works suggests that the polar PEO layer will preferentially wet the Si substrate with a native oxide layer (favourable PEO-substrate interactions) whilst PS will segregate to the air interface to form a PS-rich layer (PS has a lower surface energy, $\gamma_{PS}$ = 33 mNm-1; $\gamma_{PEO}$ = 43 mNm-1) [28-30]. As shown in Fig. 4, for the ozone-oxidized Si trenches, where the HSQ gratings were present, were engulfed with

ACCEPTED MANUSCRIPT

darker areas, suggesting that the PEO block occurred exclusively on the HSQ sidewall (prior to removal). The cylindrical PEO structures also appeared to be more inclined towards the HSQ void area. This can be explained by simple hydrophobic-hydrophilic interactions. The HSQ, after EBL exposure, formed a silica-like material which was hydrophobic in nature. When the HSQ predefined substrates were subjected to UV/Ozone treatment, the HSQ reactive sites (Si-H) were easily converted into Si−OH (silanol) by ozone [31]. Thus, the HSQ walls will bear Si-OH (making them hydrophilic) groups that can readily bond with the oxygen in PEO. Thus the hydrophobicity of the trench sidewalls plays a pivotal role in the PEO cylinder orientation of the BCP. Moreover, when the substrates were oxidized, a $SiO_2$ layer of ~ 6 nm formed the top surface layer [32]. Due to the difference in the surface energy between oxidized and HSQ etched Si surfaces, both parallel and perpendicular orientation were noticed. However, it should be noted that this phenomenon was only observed in the 90 nm pitch while wider trenches exhibited PEO dots arranged in an orderly manner. Thus, the width of the trench along with the surface chemistry was important for different nanopatterns of the BCP. The cylinder-to-cylinder spacing and the PEO cylinder diameter were also equally important so as to coordinate dot/line nanopatterns within the trenches.

On the other hand, trench width greater than 250 nm is required for parallel orientation of PEO cylinders on Ge substrates. This remarkable phenomenon observed on Ge could be attributed to the surface chemistry of Ge, which differs from that of Si. The surface of Ge is always accompanied by its native oxides, GeO and $GeO_2$. $GeO_2$ is a water soluble oxide [33], however in the BCP self-assembly procedure described here is a completely water devoid process (toluene and ethanol

ACCEPTED MANUSCRIPT

solvents). The presence of surface oxides makes the Ge surface hydrophilic in nature. The surface energy of Ge is reported to be lower than that of Si, (Ge{100} = 1.835 mN $m^{-1}$ and Si{100} = 2.130 mN $m^{-1}$) and hence the PEO block may prefer wetting the Ge surface more effectively than Si [34]. The contact angles measured for untreated GeOI were 59.6°/60.3° (left/right angle) and for citric acid treated GeOI were 54.7°/57.2°. Thus, the surface energy of untreated GeOI is 37 dyne/cm and that for citric acid treated is 41 dyne/cm. Hence, this behaviour may favour the long range parallel arrangement of the PEO block. Surface passivation method by citric acid did not particularly encourage long-range arrangement of the BCPs. Moreover, PEO cylinders, mainly parallel, as well as perpendicular to the substrate were mostly found on EBL unpatterned areas (Fig. 1c), thus confirming that Ge surface with the oxides induce parallel orientation.

As seen in all SEM images in Figs. 2 and 3, the HSQ sidewalls were preferentially wetted by the PS block (on Si and Ge). The PEO block is known to have an affinity towards the substrate interface due to being more hydrophilic than PS. The PS block, therefore, covers the free surface are, i.e. HSQ sidewalls. Si-H and Si-O bonds have been reported to be the reaction sites of HSQ [27], which can react with those on PS. The reason why more parallel alignment is observed frequently in wider Ge trenches is because of the scarce availability of SiO (HSQ) material (since the trench-width is wider). As the Ge surface area increases proportionally with the trench width, the surface energy in the confined space decreases causing an increase in the PEO affinity towards the surface and the formation of line structures. Thus, the lower surface energy of Ge in comparison to that of Si can promote long range arrangement of this BCP system. Moreover, unlike many of previously reported graphoepitaxy works, the

ACCEPTED MANUSCRIPT

study reported here does not require surface neutralisation prior to spinning down the BCP solution to induce preferential alignment. This simplifies the process by reducing one of the processing steps.

## 4. Conclusion

In summary, a DSA approach with PS-b-PEO BCP system on EBL patterned Si and Ge trenched substrate surface has been demonstrated in this report. Whilst previous DSA reports with PS-b-PEO has been demonstrated on a bare Si and Ge surface efficiently [24, 27], this article reports the BCP nanopatterns on trenched Si and Ge surfaces as there is yet limited work conducted on Ge planar surface [22, 25, 34]. Moreover, Ge can be chosen as a non-Si based alternatives due to its properties similar to Si and can be used in MOSFETs to overcome the limitations of reduced device speed [27]. Many techniques like chemical modification of the substrate surface, a brush layer or functionalization was performed to get favourable orientation and long range ordering of the BCP with respect to the substrate [35-36]. The method reported here does not require prior surface treatment, thus reducing a process step. Also, there are pattern transfer limitations to fabricate devices using polymer patterns as an etch mask can lead to device features of low aspect ratio and high line edge roughness. In this regard, iron oxide nanopatterns were used as a 'hard mask' material with high selectivity to fabricate Si and Ge device features.

The substrate surface is patterned by EBL process consisted of arrays of HSQ trenches where the width varying from 45 to 315 nm. The solvent annealing approach was applied to form different BCP nanopatterns with controlled PEO cylindrical microdomain orientation within the trenches at different temperatures and annealing times. The data shows these conditions strongly influence the formation of different nanostructures on both the substrates. On Si surfaces, the BCP mainly formed an

ACCEPTED MANUSCRIPT

orderly arrangement of arrays of nanodots with perpendicularly orientated PEO cylinders within the trenches defined by HSQ resist, whereas the non-patterned areas showed random placement of the dot structures. Ge, on the other hand, encouraged line patterns of BCP with parallel orientation of PEO domains within the wider trenches. Long range arrangement of 5, 6 and 7 parallel BCP line patterned arrays were obtained in HSQ trenches with 225, 270 and 315 nm widths, respectively. HSQ-etched Si substrate helped to achieve commendable parallel orientation of PEO within the smallest trench width of 90 nm, however, dot morphology is predominant for HSQ-etched Ge trenches for all widths. HSQ trenched Si substrate were subjected to UV/Ozone oxidation to yield an excellent DSA nanopattern arrangement throughout trenches. In the case of Ge, in an attempt to make the surface oxide-free, the substrates were treated with citric acid but this process also encouraged perpendicular cylinder formation of the PEO. Thus the native surface oxides of Ge can also be an added benefit for improved alignment of the BCP. The native oxide on Ge usually concerns for device fabrication, however in this case it proves befitting and this could be a significant progress in next generation IC technologies [38-39]. The positioning of BCP within the trenches depended on the surface and/or interfacial energies with the sidewalls of the trenches with the individual blocks of the BCP for both the substrates. In order to fabricate Si and Ge device features within trenches through the pattern transfer protocol, an in-situ metal ion inclusion technique was employed to generate iron oxide hardmask which mimics the original self-assemble BCP nanopatterns. This periodic array of nanodots and nanowires iron oxide patterns can find potential use in energy or information storage, sensing areas [37]. Further, Si and Ge nanopillars and nanowires patterned arrays with smooth and uniform sidewall throughout their entire length were fabricated through the pattern transfer process

ACCEPTED MANUSCRIPT

using ICP dry etch. However, the etch recipe was optimised for the Ge substrate to realise uninterrupted continuous nanowire patterns. An easy and robust graphoepitaxy method for fabricating Si and Ge nanopillar and nanowires arrays, which can be efficaciously used in device fabrication, is demonstrated in this article.

**Conflicts of interest**

There are no conflicts to declare.

**Acknowledgements**

The authors acknowledge the financial support from Science Foundation Ireland (SFI) under the "Novel Nanowire Structures for Devices" Project (Grant Agreement No. 09-IN1-I2602).

**References**

[1] E.-H. Lee, S.-G. Lee, O Beomhoan, S.-K. Kim. Proc. SPIE, Optoelectronics, Materials and Devices for Communications. 4580 (2001) 263.

[2] S. Stepanow, M. Lingenfelder, A. Dmitriev, N. Lin, Th. Strunskus, Ch. Wöll, J.V. Barth, K. Kern. Scientific Highlights. 2003.

[3] C.T. O'Mahony, R.A. Farrell, T. Goshal, J.D. Holmes, M.A. Morris. Thermodynamics - Systems in Equilibrium and Non-Equilibrium, Dr. Juan Carlos Moreno PirajÃ¡n (Ed.), InTech, DOI: 10.5772/20145.

[4] C. Tang, E.M. Lennon, G.H. Fredrickson, E.J. Kramer, C.J. Hawker. Science. 322 (2008) 429.

[5] T. Thurn-Albrecht, J. Schotter, G.A. Kästle, N. Emley, T. Shibauchi, L. Krusin-Elbaum, K. Guarini, C.T. Black, M.T. Tuominen, T.P. Russell. Science. 290 (2000) 2126.

[6] S.O. Kim, H.H. Solak, M.P. Stoykovich, N.J. Ferrier, J.J. de Pablo, P.F. Nealey. Nature. 424 (2003) 411.

ACCEPTED MANUSCRIPT

[7] Y. Mai, A. Eisenberg. Self-assembling of block copolymer. Chem. Soc. Rev. 41 (2012) 5969.

[8] M.C. Orilall, U. Wiesner. Chem. Soc. Rev. 40 (2011) 520.

[9] J.Y. Cheng, C.A. Ross, V.Z.-H. Chan, E.L. Thomas, R.G.H. Lammertink, G.J. Vancso. Adv. Mater. 13 (2001) 1174.

[10] Y.S. Jung, C.A. Ross. Nano Lett. 7 (2007) 2046.

[11] T. Thurn-Albrecht, R. Steiner, J. DeRouchey, C.M. Stafford, E. Huang, M. Bal, M. Tuominen, C.J. Hawker, T.P. Russell. Adv. Mater. 12 (2000) 787.

[12] S.Y. Yang, I. Ryu, H.Y. Kim, J.K. Kim, S.K. Jang, T.P. Russell. Adv. Mater. 18 (2006) 709.

[13] I. Bita, J.K.W. Yang, Y.S. Jung, C.A. Ross, E.L. Thomas, K.K. Berggren. Science. 321 (2008) 939.

[14] S. Xiao, X.M.Yang, E.W. Edwards, Y.-H. La, P.F. Nealey. Nanotechnology 16 (2005) S324.

[15] S.-J. Jeong, J.Y. Kim, B.H. Kim, H.-S. Moon, S.O. Kim. Mater. Today. 16 (2013) 468.

[16] D. Borah, S. Rassapa, M.T. Shaw, R.G. Hobbs, N. Petkov, M. Schmidt, J.D. Holmes, M.A. Morris. J. Mater. Chem. C. 1 (2013) 1192.

[17] X.M. Yang, S. Xiao, Y. Hsu, M. Feldbaum, K. Lee, D. Kuo. J. Nanomater. Article ID 615896 (2013) 17.

[18] J.G. Son, J.-B. Chang, K.K. Berggren, C.A. Ross. Nano Lett. 11 (2011) 5079.

[19] D.O. Shin, B.H. Kim, J.-H. Kang, S.-J. Jeong, S.H. Park, Y.-H. Lee, S.O. Kim. Macromolecules. 42 (2009) 1189.

[19] T. Ghoshal, R. Senthamaraikannan, M.T. Shaw, J.D. Holmes, M.A. Morris. Nanoscale. 4 (2012) 7743.

ACCEPTED MANUSCRIPT

[20] M.A. Morris, D. Borah, T. Ghoshal, P. Mokarian. Google patent. EP 2594995 A1, October 15, 2013.

[21] T. Wahlbrink, T. Mollenhauer, Y.M. Georgiev, W. Henschel, J.K. Efavi, H.D.B. Gottlob, M.C. Lemme, H. Kurz, J. Niehusmann, P. Haring Bolivar. Microelectron. Eng. 78 (2005) 212.

[22] C. Cummins, R.A. Kelly, A. Gangnaik, Y.M. Georgiev, N. Petkov, J.D. Holmes, M.A. Morris. Macromol Rapid Commun. 36 (2015) 762.

[23] Y.-K. Hong, D.-H. Eom, S.-H. Lee, T.-G. Kim, J.-G. Park, A.A. J. Electrochem. Soc. 151 (2004) G756.

[24] T. Ghoshal, M.T. Shaw, C.T. Bolger, J.D. Holmes, M.A. Morris. J. Mater. Chem. 22 (2012) 12083.

[25] C. Cummins, A. Gangnaik, R. Kelly, A. Hydes, J. O'Connell, N. Petkov, Y.M. Georgiev, D. Borah, J.D. Holmes, M.A. Morris. J. Mater. Chem. C. 27 (2015) 6091.

[26] R.G. Hobbs, R.A. Farrell, C.T. Bolger, R.A. Kelly, M.A. Morris, N. Petkov, J.D. Holmes. ACS Appl. Mater. Interfaces. 4 (2012) 4637.

[27] T. Ghoshal, T. Maity, R. Senthamaraikannan, M.T. Shaw, P. Carolan, J.D. Holmes, S. Roy, M.A. Morris. Sci Rep. 3 (2013) 2772.

[28] R.A. Farrell, N. Petkov, M.A. Morris, J.D. Holmes. J. Colloid Interface Sci. 349 (2010) 449.

[29] R.A. Farrell, T.G. Fitzgerald, D. Borah, J.D. Holmes, M.A. Morris. Int. J. Mol. Sci. 10 (2009) 3671.

[30] L. Spialter, L. Pazdernik, S. Bernstein, W.A. Swansiger, G.R. Buell, M.E. Freeburger. J. Am. Chem. Soc. 93 (1971) 5682.

[31] C.K. Fink, K. Nakamura, S. Ichimura, S.J Jenkins. J. Phys.: Condens. Matter. 21 (2009) 183001-1-19.

ACCEPTED MANUSCRIPT

[32] P.W. Loscutoff, S.F. Bent. Annu. Rev. Phys. Chem. 57 (2006) 467.

[33] R. J. Jaccodine. J. Electrochem. Soc. 110 (1963) 524.

[34] C. Cummins, T. W. Collins, R. A. Kelly, E. McCarthy, M. A. Morris. Nanotechnology 27 (2016) 484003.

[35] S. B. Darling, Prog. Polym. Sci. 32 (2007) 1152.

[36] A. P. Marencic, R. A. Register. Annu. Rev. Chem. Biomol. Eng. 1 (2010) 277.

[37] L. Pan, H, Qiu, C. Dou, Y. Li, L. Pu, J. Xu, Y. Shi, Int. J. Mol. Sci. 11 (2010) 2636.

[38] T. Akatsu, C. Deguet, L. Sanchez, F. Allibert, D. Rouchon, T. Signamarcheix, C. Richtarch, A. Boussagol, V. Loup, F. Mazen, J. M. Hartmann, Y. Campidelli, L. Clavelier, F. Letertre, N. Kernevez, C. Mazure, Mater. Sci. Semicond. Process. 9 (2006) 444.

[39] K. Kita, T. Takahashi, H. Nomura, S. Suzuki, T. Nishimura, A. Toriumi, Jpn. J. Appl. Phys. 47 (2008) 2349.

ACCEPTED MANUSCRIPT

ACCEPTED MANUSCRIPT

**Figure Captions:**

Scheme 1: Schematic description of the graphoepitaxy process for the fabrication of Si and Ge trenches on substrate surface and the fabrication of Si and Ge nanopatterns within the trenches via BCP hard mask inclusion technique.

Fig. 1. (a) Array of 50 nm wide HSQ lines with a 135 nm trench size prior to BCP processing and (b) BCP arrangement on an open surface area of a Si substrate (c) self-assembly on Ge surface.

Fig. 2. SEM images of DSA on the two substrates, processed at various conditions (a) solvent annealed at 50 °C for 1.30 h on Si/90 nm (HSQ trench width), (b) at 60 °C for 2h on Si/135 nm (c) at 50 °C for 1.30 h on Ge/225 nm (d) at 50 °C for 2h on Ge/315 nm.

Fig. 3. SEM images of the BCP DSA in trenches that were etched into the substrates using the HSQ mask (a) 90nm wide trenches in Si (b) 270 nm in Si (c) 135 nm in Ge and (d) 270 nm in Ge.

Fig. 4. SEM images of BCP nanopatterns after UV/Ozone treatment of HSQ-defined Si substrates after solvent annealing at 60 °C for (a) 1.5 h and (b) 2 h. Pattern degeneration or swelling is shown by the red circles.

ACCEPTED MANUSCRIPT

ACCEPTED MANUSCRIPT

Fig. 5. SEM images of a Ge surface treated with 1 M citric acid prior to BCP processing. DSA of the PEO cylinders in (a) open area showing perpendicular orientation of PEO cylinders, (b) 135 nm HSQ trench and (c) 270 nm HSQ trench.

Fig. 6. SEM images of hexagonal ordered oxide nanodots and lines after UV/Ozone treatment on (a) an unpatterned Ge area and (b) 135 nm HSQ trenches on Si; (c) 315 nm HSQ trench on Ge surface.

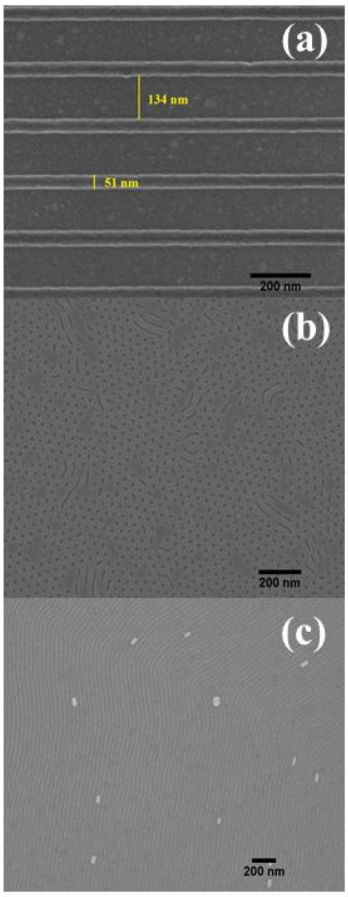
Fig. 7. (a) SEM image of Si nanopillars formed after pattern transfer through ICP etch within 180 nm wide HSQ guided Si trenches, (inset) tilted SEM images showing height Si nano pillars and (b) high resolution TEM cross-sectional image of the Si nanopillars with iron oxide nanodots at top.

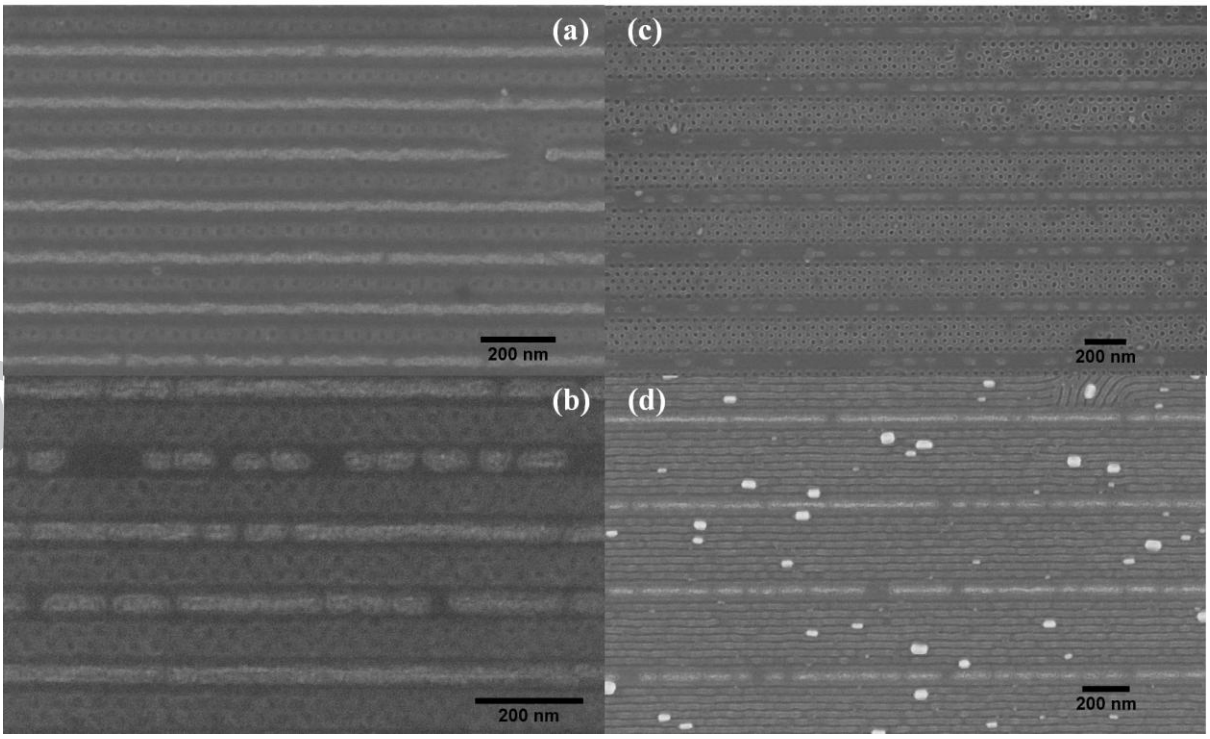
Fig. 8. SEM images of nanopatterns formed after pattern transfer into HSQ guided Ge trench through the iron oxide hard mask with ICP etch time (a) 9 s (180 nm trench width), (b) 6 s (225 nm trench width), (c) 4s (315nm trench width). Insets in show etched morphologies on unpatterned areas.

Fig. 9. Ge Line patterns formed after pattern transfer with $C_4F_8$ gas for 9s on (a) SEM image of 135 nm wider trench and (b) cross sectional TEM image of 4 arrays of Ge nanowire with HSQ and iron oxide at top.

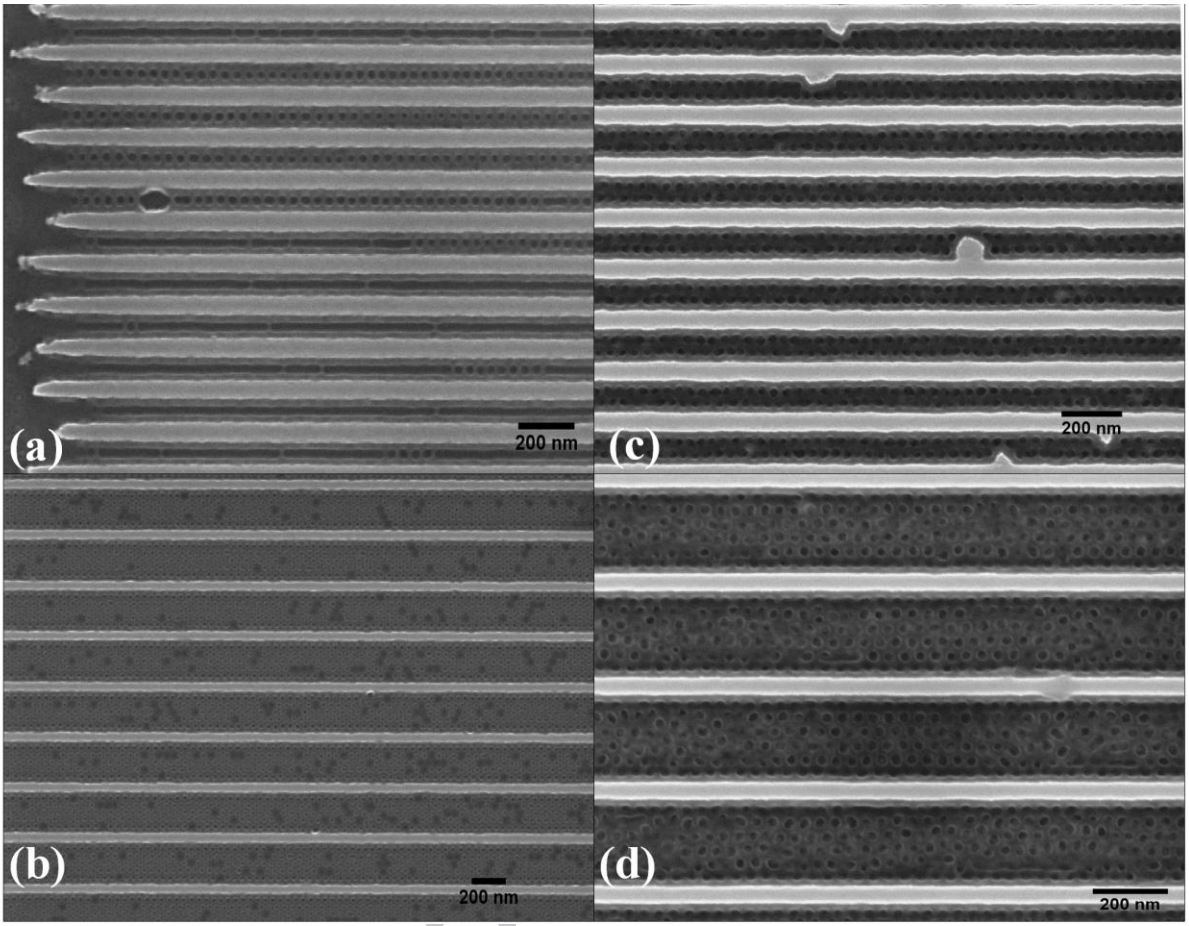
ACCEPTED MANUSCRIPT

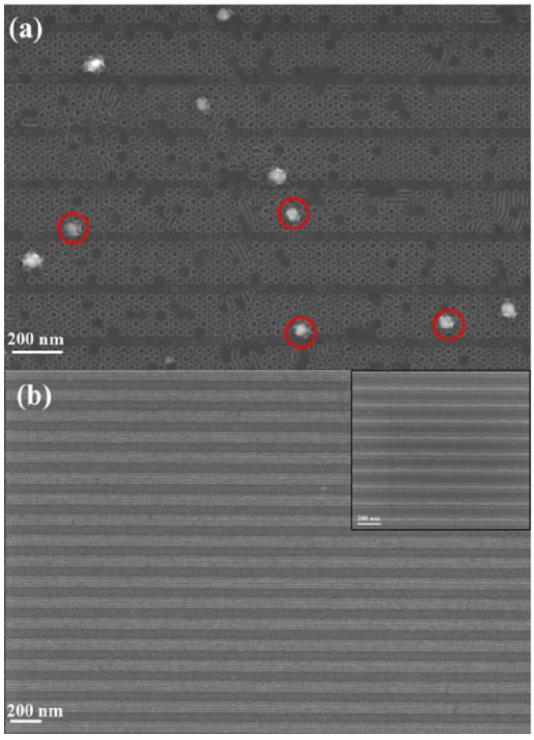
ACCEPTED MANUSCRIPT



ACCEPTED MANUSCRIPT



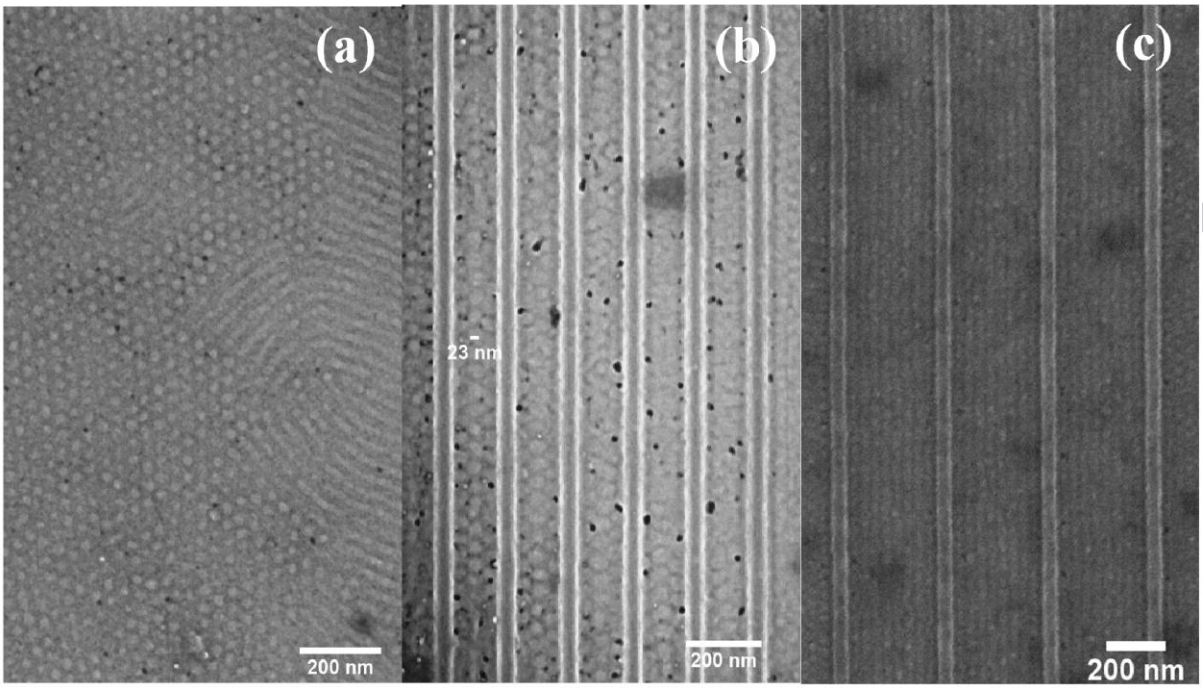



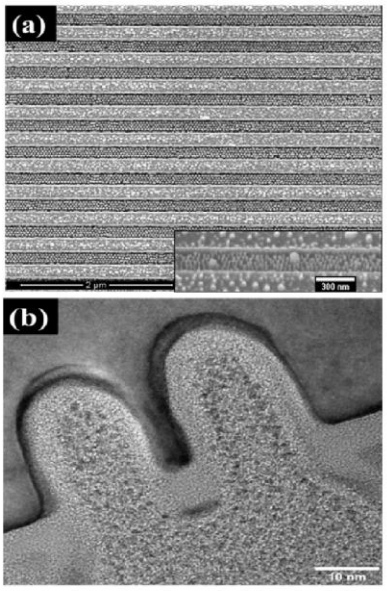
ACCEPTED MANUSCRIPT



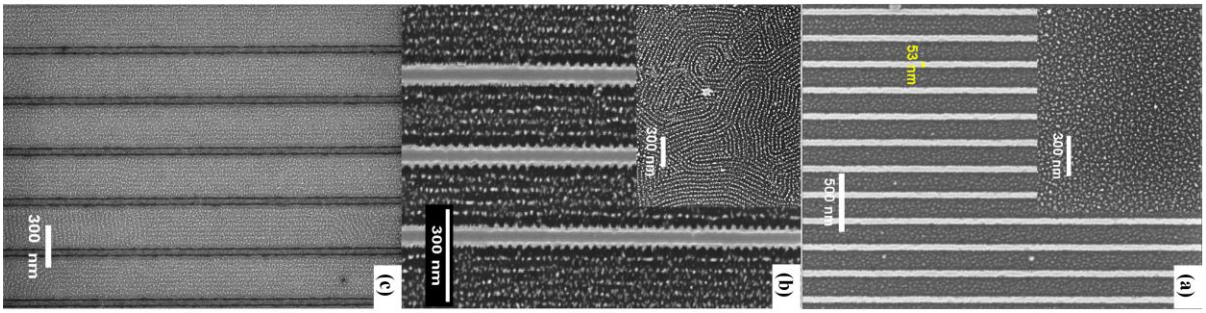

ACCEPTED MANUSCRIPT

ACCEPTED MANUSCRIPT



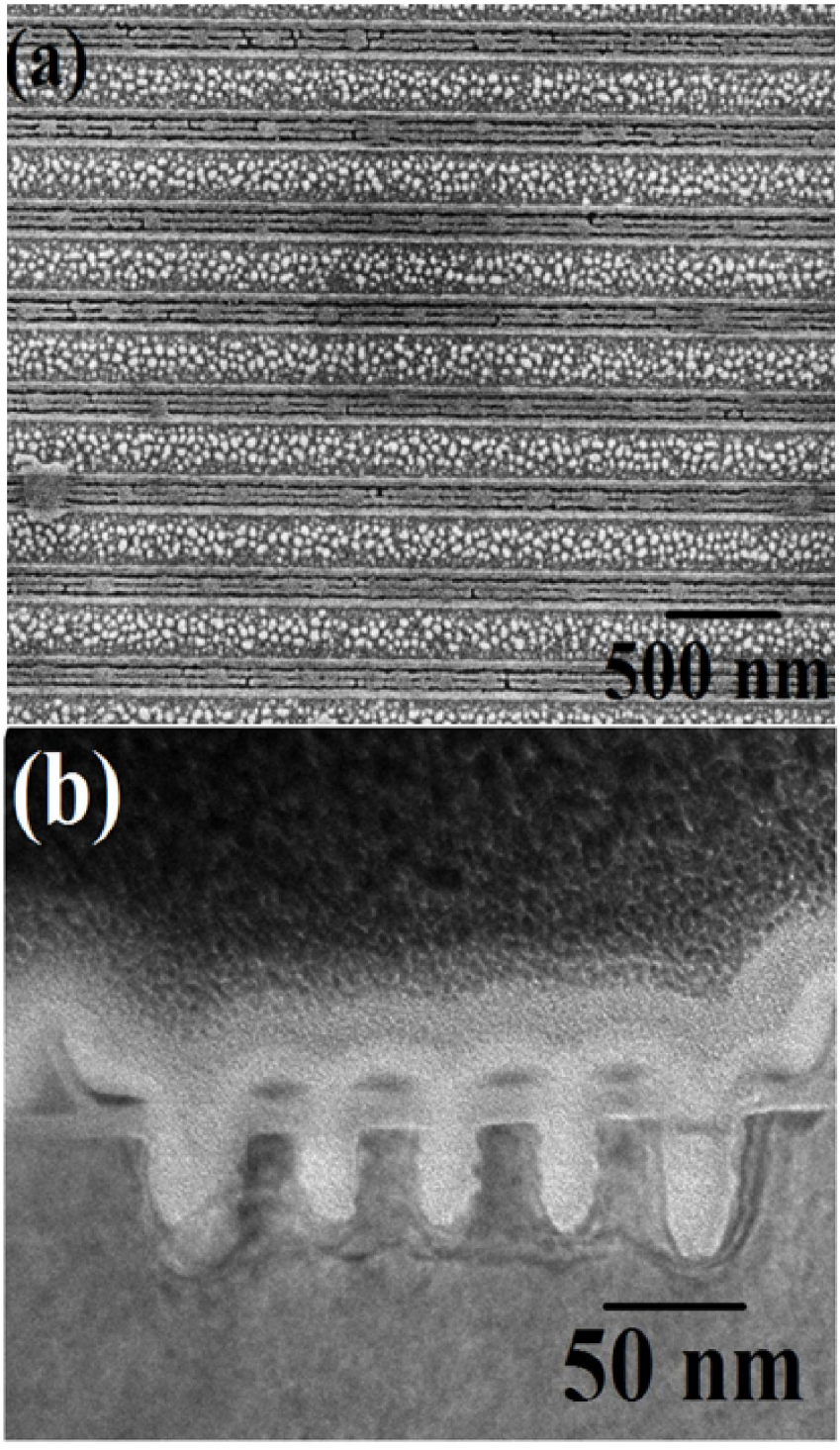



ACCEPTED MANUSCRIPT

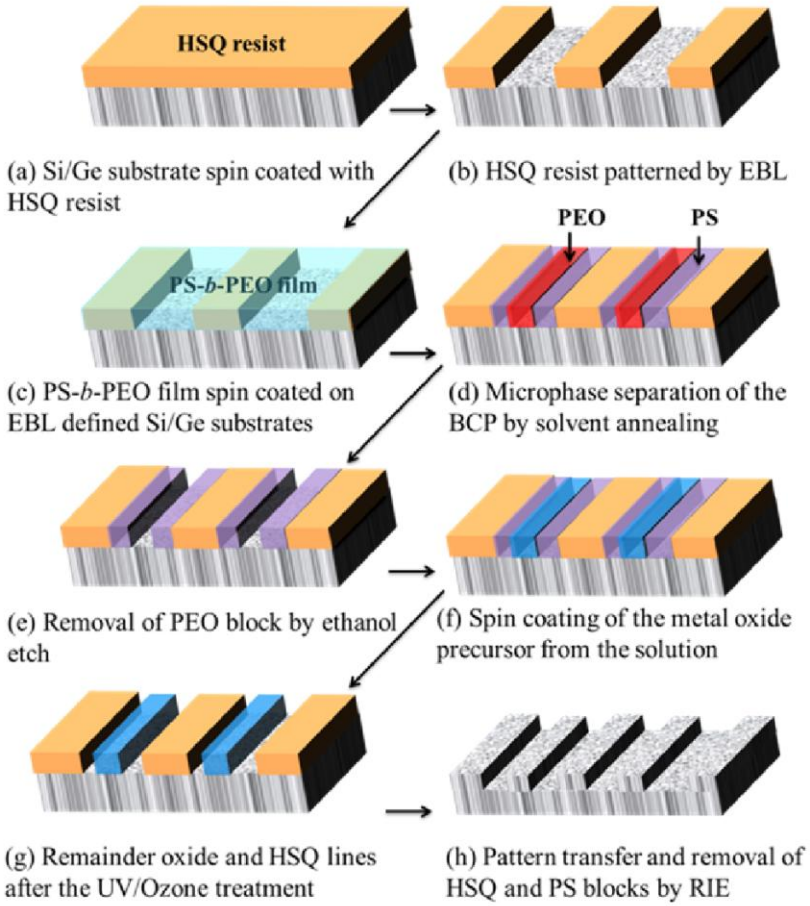



ACCEPTED MANUSCRIPT

ACCEPTED MANUSCRIPT



ACCEPTED MANUSCRIPT




ACCEPT

ACCEPTED MANUSCRIPT

